Integrated Nano, 2024, Vol. 1, Iss. 1, 48-59

DOI: 10.62184/in.jin010420245

Research Article

SCIENCE PARK PUBLISHER

Integrated Nano

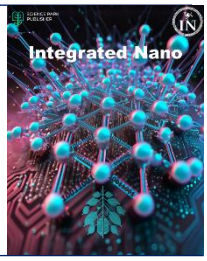

Down and Upconversion NGQDs and CuInS/ZnS QDs Nanocomposite for Ascorbic Acid Sensing

Rania Adel[1,*], Shaker Ebrahim[1], Moataz Soliman[1], Marwa Khalil[2]

[1] Materials Science Department, Institute of Graduate Studies and Research, Alexandria University, P.O. Box 832, Alexandria, Egypt

[2] Composite and Nanostructured Materials Research Department, Advanced Technology and New Materials Research Institute, City of Scientific Research and Technological Applications (SRTA-City), New Borg Elarab City, P.O. Box 21934 Alexandria, Egypt

Received: 21, 09, 2024; Accepted: 05, 11, 2024; Published: 11, 11, 2024

Abstract

Copper indium sulfide/zinc sulfide (CuInS/ZnS) QDs and Nitrogen graphene quantum dots (NGQDs) were synthesized via aqueous solution methods and facile hydrothermal, respectively. Herein, according to the photoluminescence (PL) properties of QDs, a fluorescent nanocomposite of CuInS/ZnS QDs and NGQDs was synthesized. This nanocomposite was characterized by high-resolution transmission electron microscopy (HRTEM) and PL spectroscopy. This fluorescent nanocomposite was developed as a highly sensitive and selective ascorbic acid optical biosensor based on the luminescent quenching in the range from 10 to 500 µM with a correlation coefficient (R^2) of 0.9964 and limit of detection (LOD) of 16.8 µM. HRTEM micrographs confirmed the preparation of CuInS/ZnS QDs with an average diameter size of 3 nm and NGQDs with an average diameter size of 5 nm.

Keywords: Nanocomposite; Quantum Dots; Upconversion; Photoluminescence; Ascorbic Acid

1. Introduction

Ascorbic acid (AA) presented in vegetables and fruits is important for the building of the human body [1-3].

AA deficiency can cause scurvy, hyperacidity, hypoimmunity and coronary heart. Therefore, it is necessary to find a fast, accurate, sensitive and low-cost method to determine AA [3].

QDs have been exploited in many applications due to special properties such as quantum confinement, upconversion PL, and a wide range of emission spectra such as bioimaging, [4] light emitting diode (LED) [5] and biosensors [6-7]. CuInS QDs are considered as a ternary semiconductor compound and belong to the I-III-VI_2 family and It is free of any toxic metal ions. The band gap energy of CuInS is about 1.55 eV [8-9]. CuInS/ZnS QDs cover a wide range of PL emissions from visible regions to near-infrared regions. The synthesis of heteroatoms such as P, S, F, B, and N-doped GQDs increases the attraction. Empirical results prove that nitrogen atom is improving the properties of GQDs [10-11].

The upconversion PL occurs when the energy photon of excitation is lower than the emission. Widespread observation of the upconversion PL has been made in a variety of materials, including semiconductor QDs [12-13].

For the detection of AA. They reported that the PL intensity of CuInS QDs increased directly with increasing concentration of AA at pH 7.4. The PL spectra enhancements were caused by the chelating and properties reducing of AA and the detection of AA was from 0.25 to 200 mmol L^{-1} [14].

Integrated Nano, 2024, Vol. 1, Iss. 1, 48-59
DOI: 10.62184/in.jin010420245

Research Article

Hossein Safardoust-Hojaghan et al. prepared S, NGQDs via a simple hydrothermal method. The designed sensor depended on an "on-off" mode for detection by adding copper ion to quench S, NGQDs (off) and then adding different concentrations of AA that reacted with copper ion and enhancing the PL of S, NGQDs with increasing concentration of AA. The concentration range of AA was ranged from 10 to 500 μM and the limit of detection is observed at 1.2 μM [15].

Chunxia Wang et al. synthesized NGQDs by chemical oxidation of 3-dimension nitrogen-doped porous graphene frameworks. NGQDs were incorporated with cobalt oxide hydroxide (CoOOH) nanosheets to sense AA. CoOOH nanosheets could act as the quencher for NGQDs due to the absorption of $CoCl_2$. The reaction mechanism was reduced CoOOH nanosheets to Co^{2+} while the AA was oxidized to dehydroascorbic acid and detection concentration of AA with the LOD up to 1.85 mM [16].

Our work strategy includes the synthesis of NGQDs, CuInS/ZnS QDs, NG/CuInS/ZnS QDs, and nanocomposites in different ratios. Upconversion phenomena for the prepared QDs are investigated and discussed. A cheaper and simpler biosensor based on NG/CuInS/ZnS QDs nanocomposite for AA detection is the main target with different AA concentrations and different incubation times.

2. Materials and Methods

2.1. Materials

Copper chloride anhydrous ($CuCl_2$) (99%), indium (III) chloride tetrahydrate ($InCl_3.4H_2O$) (97%), and 3-mercaptopropionic acid (MPA) (99%) were purchased from Across Organic Company, Belgium. Citric acid was purchased from Luba-chem. Urea was supplied from Elnasr Company, Egypt. pH 7 phosphate buffer solution and Sodium sulfide (Na_2S) were purchased from Chem-lab, Belgium. Zinc acetate dihydrate ($Zn(Ac)_2.2H_2O$) (98.5%) was purchased from Oxford Company, India. Ethanol (99.9%) was supplied by International Company for Sup. & Med. Industries. Isopropanol (99.5%) was supplied from Alalamia Company, Egypt. Sodium hydroxide (NaOH) was supplied from Elnasr Company, Egypt. Hydrochloric acid (HCl) was supplied from Fischer Company, Germany. AA was supplied by the pharmacy.

2.2. Synthesis of CuInS/ZnS QDs

CuInS/ZnS QDs were synthesized as following steps. Briefly, 0.6 mL of $InCl_3 \cdot 4H_2O$ stock solution (0.1 M) was dissolved in 10 mL deionized water with 1 mL MPA (4.5 M). In a separate flask containing $CuCl_2$ (0.1 mL, 0.1 M) with 0.5 mL MPA (4.5 M) dissolved in 10 mL deionized water and the pH was adjusted to 9.0 by using 1M NaOH to remove turbidity of the solution. The solution of $CuCl_2$ was injected into $InCl_3$ solution with a continuous stirring for 2 min to produce a molar ratio of Cu^{2+} to In^{3+} of 1:6. Subsequently, Na_2S solution (0.5 mL, 0.04 mmol) was injected into the above mixture at room temperature with a vigorous stirring for 5 min. The latter mixture was heated to 90 °C for 30 min and then 1 mL of 0.04 M $Zn(Ac)_2.2H_2O$ was dropwise to this mixture with a continuous stirring for another 5 min to obtain CuInS/ZnS QDs. The color of the reaction mixture progressively changed from yellowish to brown.

CuInS QDs powder was obtained by dissolving in isopropanol with the ratio 1:0.5 and centrifuged at 6500 for 15 minutes and dried in air to get (0.448 mg/mL).

2.3. Preparation of NGQDs

NGQDs were prepared by using 3.15 g of citric acid and 2.7g of urea were dissolved in 75 mL DI water and stirred for 5 minutes up to the formation of a clear solution then it was transferred into 250 mL Teflon lined stainless autoclave and kept in the oven for 4 hours at 160°C.

NGQDs powder was obtained by adding ethanol to NGQDs with a ratio of 2:1 in the centrifuge for 10 minutes at 6000 rpm washing the residual 3 times and drying in a vacuum oven at 60°C to obtain fine powder (10 mg /mL).

2.4. Preparation of NG/CuInS/ZnS QDs

The formation of NG/CuInS/ZnS QDs nanocomposite was synthesized physically by mixing CuInS/ZnS QDs with NGQDs at a ratio (0.5:1) and shaking for 30 minutes. The nanocomposite

Integrated Nano, 2024, Vol. 1, Iss. 1, 48-59
DOI: 10.62184/in.jin010420245

Research Article

of ratio (1:0.5) was purified with isopropanol at 3000 rpm for 15 minutes.

2.5. Characterization

To examine the emission properties, PL spectra were recorded by using a Perkin Elmer (LS-55) fluorescence spectrometer, and the samples were dispersed in DI water.

The morphological properties were examined using HR-TEM images obtained with a JEOL JEM 2100F microscope at an accelerating voltage of 200 kV. For HRTEM sample preparation, the dried QD powder was dispersed in ethanol, and a drop of this dispersion was placed onto a 3 mm diameter carbon-coated copper grid. The grid was then air-dried before imaging.

2.6. Detection of AA

A 4.5 mM solution of AA was prepared by using 17.6 mg in 100 mL of deionized water. 70 µL nanocomposite was added to different concentrations of AA from 10 µM to 500 µM and 2mL phosphate buffer (pH=8) buffer followed by incubation for 10 minutes. For analytical parameters optimization, the slope of the calibration curve was used based on equation (1).

$$\frac{F^\circ - F}{F^\circ} = a\,C_{AA} + b \qquad (1)$$

where F° and F represent the PL intensity of NG/CuInS/ZnS QDs in the absence and presence of AA, a and b refer to the slope and the intercept of the calibration curve, respectively.

The limit of detection (LOD) of the bioanalyte molecule was estimated from the following equation (2).

$$LOD = \frac{3SD}{s} \qquad (2)$$

Where SD is the standard deviation and S is the slope of the curve.

3. Results and Discussion

3.1. Morphological properties

HRTEM images of NGQDs, CuInS/ZnS QDs, and NG/CuInS/ZnS QDs nanoparticles are shown in Figure 1. It is observed that the size of NGQDs with an average diameter of about 5.30-8.30 nm and well-defined lattice fringes with an interplanar spacing of about 0.24 nm attributed to (100) is shown in the inset of the Figure 1 [10, 17-20].

Moreover, HRTEM images of CuInS/ZnS QDs are estimated to be in the range of 3.18-4.57 nm and appear highly crystalline. Also, the interplanar spacings are 0.31 nm for the (112) plane [21-24]. It is observed that some nanoparticles are uniformly distributed and separated from each other, while others are hybridized into agglomerates. The isolated particles could be identified as the average size of CuInS/ZnS QDs are 4.5 nm and 6 nm for NGQDs. Regarding the hybridized particles, two different types of lattice spacing corresponding to the 0.35 nm of CuInS/ZnS QDs and the 0.26 nm of NGQDs are detected. This indicates that CuInS/ZnS QDs and NGQDs and are tightly combined [25].

3.2. Optical properties of NGQDs, CuInS/ZnS, and NG/CuInS/ZnS QDs nanocomposite

To investigate the optical properties of emission, PL spectra of NGQDs, CuInS/ZnS QDs, and NG/CuInS/ZnS QDs are carried out at excitation wavelength 350 nm as depicted in Figure 2. PL spectra of CuInS/ZnS QDs and NGQDs are showen at 640 and 440 nm respectively. According to nanocomposite QDs, the PL spectra show a decrease in the emission peak of NGQDs and a slightly red shift of the peak with about 3 nm and also complete quenching of the emission of the CuInS/ZnS QDs as the same charge transfer process between CuInS/ZnS QDs and NGQDs. It is shown that the full-width half-width (FWHM) of NG/CuInS/ZnS QDs nanocomposite was reported to be 98 nm while for NGQDs it is 80 nm which detects recombination in the hybrid structures of NGQDs and CuInS/ZnS QDs. NGQDs are bound to the surface of the CuInS/ZnS QDs and serve as ligands beside MPA [26-27]. In addition, NGQDs may be bonded with the carboxylate groups of MPA and lead to charge transfer between NGQDs [28-30].

Integrated Nano, 2024, Vol. 1, Iss. 1, 48-59

DOI: 10.62184/in.jin010420245

Research Article

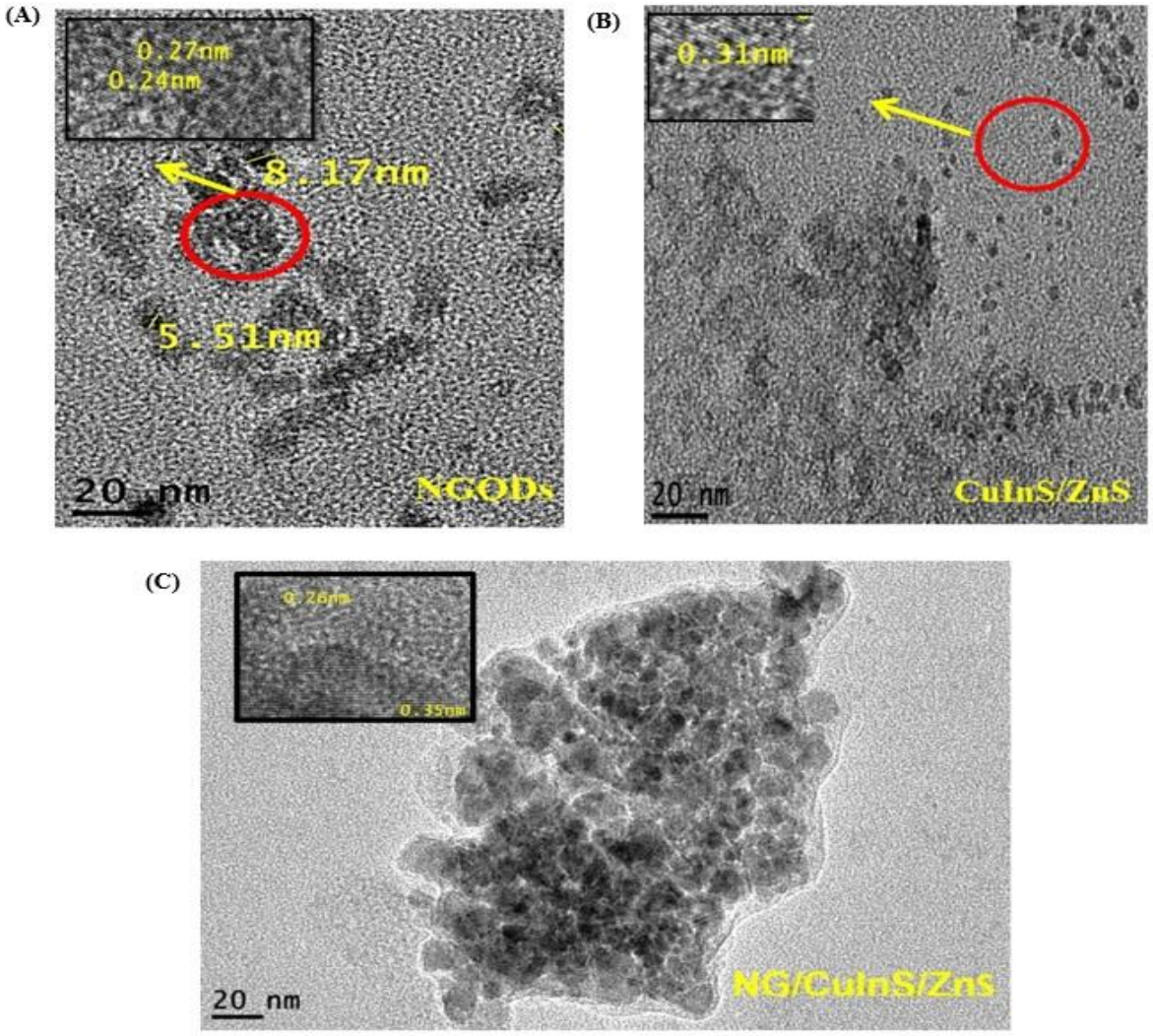

Figure 1. HRTEM images of NGQDs (A), CuInS/ZnS QDs (B) and NG/CuInS/ZnS QDs nanocomposite (C).

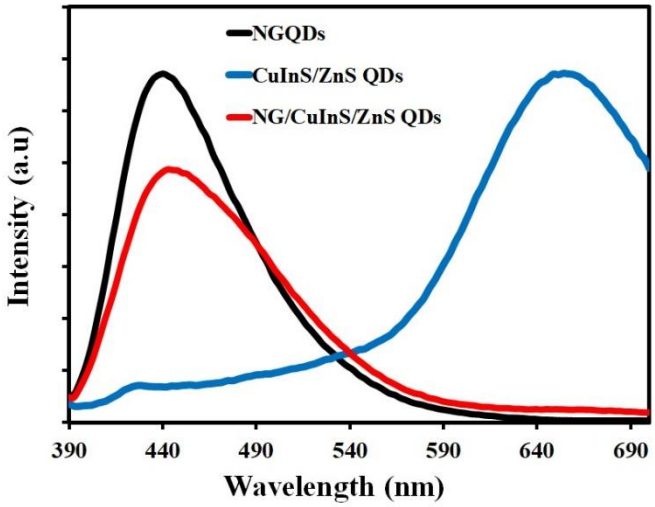

Figure 2. PL spectra of NGQDs, CuInS/ZnS QDs, and NG/CuInS/ZnS QDs nanocomposite excitation 350 nm.

Integrated Nano, 2024, Vol. 1, Iss. 1, 48-59

DOI: 10.62184/in.jin010420245

Research Article

3.3. Upconversion PL of QDs

In Figure 3.A, the upconversion PL spectra of NGQDs excited by long-wavelength from 650 to 800 nm are observed. The upconversion emission that appeared at 450 nm is shifted by 7 nm compared to the downconversion peak [31]. The upconversion emission intensity of NGQDs shown in the inset of Figure 3.A shows a linear increase in emission at the higher excitation wavelength of 750 nm and then the intensity decreases again at excitation 800 nm [32]. The most probable mechanism for the upconversion emission of NGQDs is multi-photon absorption.

The luminescence of NGQDs originates from the π –π electron transition since NGQDs have a large π conjugated system. Furthermore, the lone pair electrons in the amine group act as a donating group which are doped in the aromatic ring of NGQDs and form p−π conjugation for enlarging the π-conjugated system. Also, the strong orbital interaction between amine bonding and the π-conjugated system of the NGQDs elevates the primary highest occupied molecular orbitals (HOMO) to a higher orbit. This results in facilitating the charge transfer and enhancing the two-photon excitation [33]. The upconverted PL is an anti-stokes transition. Specifically, when the π orbital electrons are excited by low-energy photons, the π electrons will move to a high-energy state such as LUMO, and then the electrons return to the low-energy state of the σ orbital as shown in Figure 3.B [34]. The energy levels of π and σ orbitals are provided by the carbene ground-state multiplicity. The multiplicity of the carbene ground-state is equal to the difference in energy between the π and σ orbitals [35]. Hence, strong two-photon-induced luminescence can be observed. The increase of excitation peak from 650 to 800 nm leads to a shift in the emission peak of upconversion slightly to longer wavelength as anti-Stokes type emission [36].

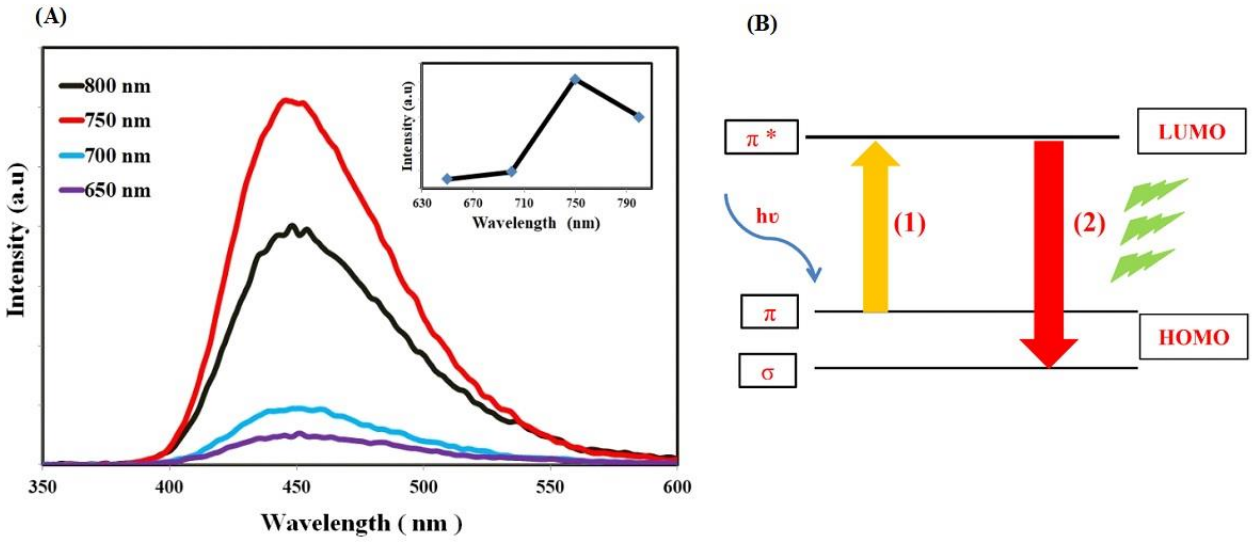

Figure 3. Upconversion PL spectra of NGQDs with different excitations, inset: PL intensity vs excitations wavelength (A), Schematic diagram of upconversion PL of NGQDs; (1) lower energy absorption and (2) higher energy upconversion emission (B).

Figure 4 displays the upconversion PL spectra of CuInS QDs at different excitation wavelengths from 730 nm to 800 nm. The upconversion and downconversion emissions are similar concerning the PL peak that appears at 650 nm. This emission peak is enhanced with increasing excitation wavelength from 730 to 800 nm and it is found that the linear correlation coefficient (R^2) equals 0.99 and the sensitivity is 1.6/nm as shown in the inset of Figure.

The surface of CuInS/ZnS QDs is passivated by a large amount of electron-donating groups such as sulfur present in MPA,

Integrated Nano, 2024, Vol. 1, Iss. 1, 48-59

DOI: 10.62184/in.jin010420245

Research Article

COOH, and ZnS. This passivation layer on the surface of CuInS/ZnS QDs creates the donation of electrons to the QDs and leads to increased electron density on the surface. It is observed that the cascade photon absorption mechanism for this conversion is dominant due to the location of the MPA HOMO level (-6.7eV) lower than that of ZnS (-6.8 eV) [37-38]. The formation of QDs with MPA ligands results in the formation of a trap state located in the conduction band of the ZnS shell. The formation of an exciton in the charge-transfer transition between the molecule HOMO of MPA and ZnS. The electron tends to be localized in the QDs core. On the other hand, the hole is trapped in the HOMO of the ligand, additional low-energy photon absorption may excite this trapped hole even more, causing it to recombine with the electron in the CuInS core as illustrated in Figure 4.B [39].

Another photon upconversion mechanism is an anti-Stokes process in which photon absorption produces a re-emission with an energy higher than the excitation energy [40-41]. When atoms absorb energy and transfer from the ground state to the E1 level, equal or different atoms rise from the E1 state to the higher excited state E2. This results in upconversion emission until these excited atoms fall to the ground and another photon emits upconversion fluorescence as shown in Figure 4.C [40].

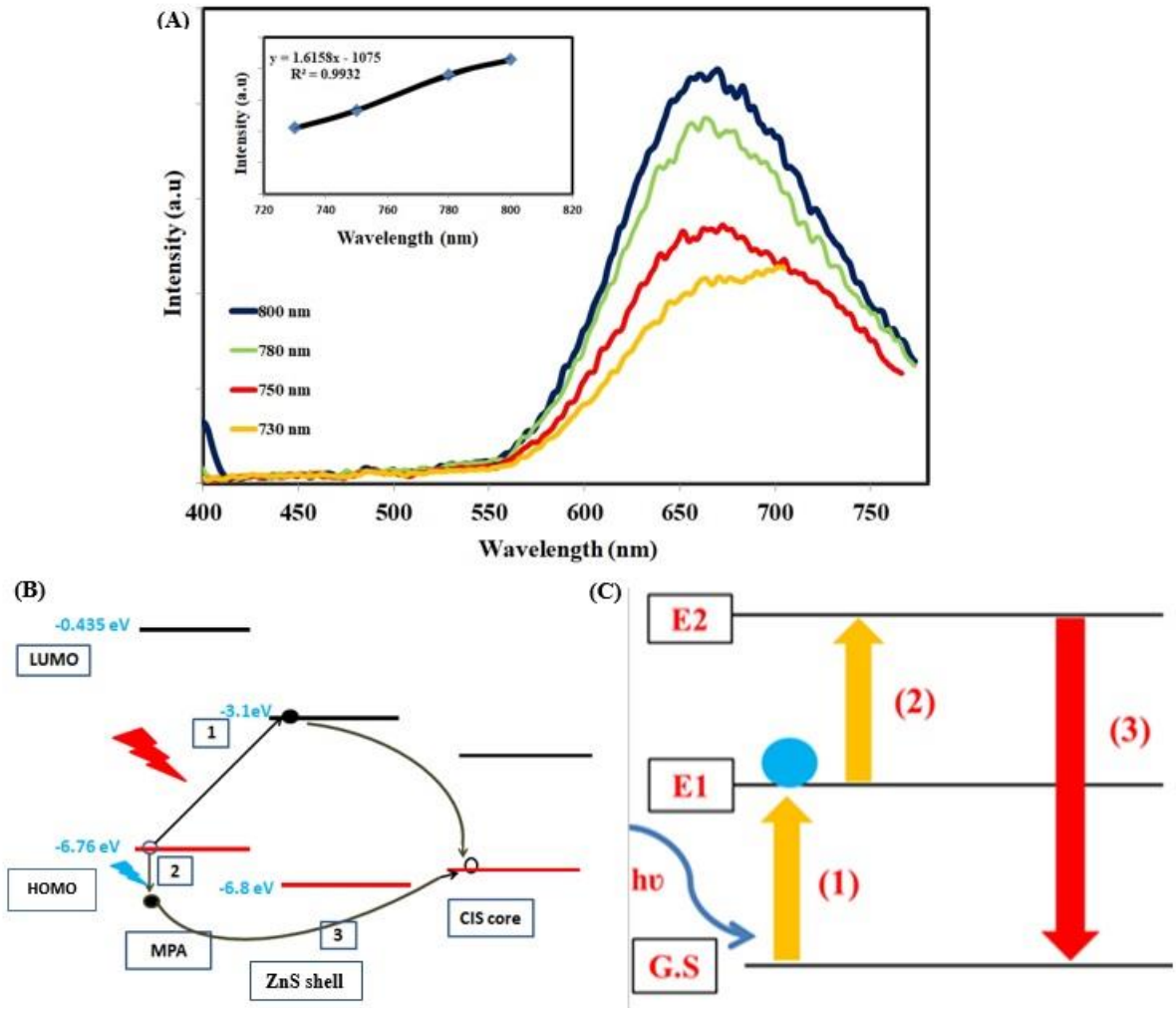

Figure 4. Upconversion PL spectra of CuInS/ZnS QDs nanocomposite at different excitation wavelength, inset: the plot of the PL intensity and relative excitation of CuInS/ZnS QDs (A), Schematic illustration of QD-ligand band alignment and conversion process by sequential photon absorption (B), Schematic representation of upconversion process (1, 2) The lower energy absorption and (3) Higher energy upconversion emission (C).

Integrated Nano, 2024, Vol. 1, Iss. 1, 48-59
DOI: 10.62184/in.jin010420245

Research Article

On the other hand, the upconversion PL spectra of NG/CuInS/ZnS QDs nanocomposite appear as an emission at 640 nm as CuInS/ZnS QDs. The intensity of the PL excitation increases from 730 to 800 nm as shown in Figure 5. The upconversion PL spectrum of NG/CuInS/ZnS QDs appears at 650 nm while the downconversion PL spectrum is at 443 nm. It is indicated that CuInS/ZnS QDs are domain in upconversion PL while NGQDs are completely quenched. This emission peak is enhanced with increasing excitation wavelength from 730 to 800 nm and it is found that R^2 equals 0.98 and the sensitivity is 1.15/nm as shown in the inset of Figure 5 [22]. There are two methods for quenching semiconductor QDs emission. First, rather than acting as MPA, the NGQDs function as ligands because they are attached to the surface of the CuInS/ZnS QDs. Second, NGQDs and CuInS/ZnS QDs may form a bond through the carboxylate group in MPA, which would allow energy to be transferred between the two. In this way, NGQDs and MPA can function as a capping on the CuInS core. The findings imply that a lower CuInS/ZnS ratio of 0.5 promotes and produces an optimum fluorescence in the nanocomposite [22].

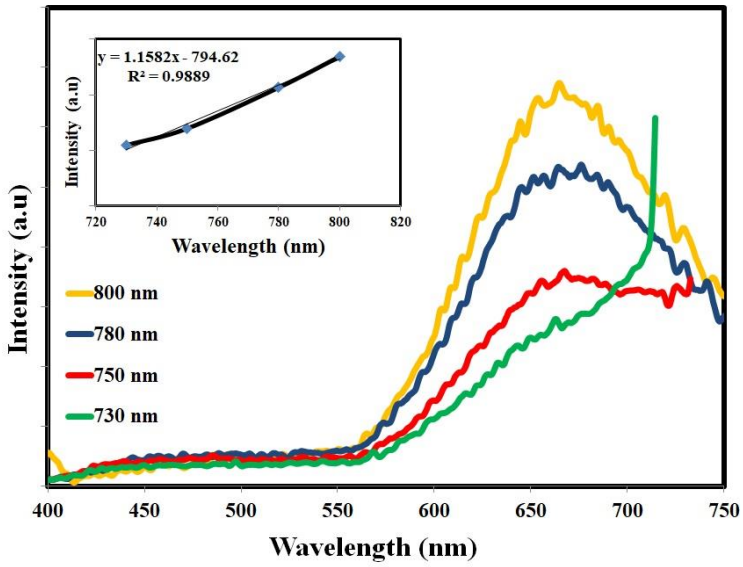

Figure 5. Upconversion PL spectra of NG/CuInS/ZnS QDs nanocomposite at different excitation wavelengths, inset: the plot of the PL intensity and relative excitation of NG/CuInS/ZnS QDs nanocomposite.

3.4. NG/CuInS/ZnS QDs probe for AA

As a radical scavenger, AA can quench QDs. The ribose ring of AA oxidizes, acting as a hole trap to quench QD fluorescence. When electrons transfer from the QDs' CB to AA, intermediate AA ions form. AA can lose a hydrogen ion due to the stability of phenoxide and ascorbate ions.

3.4.1. Effect of incubation time

The incubation time of AA with NG/CuInS/ZnS QDs illustrated in Figure 6 indicates the reaction between AA and nanocomposite occurs rapidly and PL intensity is quenched rapidly within 10 minutes and then the PL is fixed until 40 minutes. The optimal incubation time of 10 minutes is employed in further experiments.

3.4.2. Effect of pH of NG/CuInS/ZnS QDs with AA

The PL spectra of NG/CuInS/ZnS QDs with AA at different pH from 6 to 10 at the same concentration of 100 μM are shown in Figure 7. The weak intensity of the quantum dots is observed at pH 6, 8, and 10. The PL intensity of the NG/CuInS/ZnS QDs–AA mixture solution increases slightly as the pH level changes from 6 to 10. Considering the protonation of the QDs in an acidic medium, AA decomposes in an alkaline solution and is easily oxidized, and the physiological condition of pH 8 is used in further experiments [14].

Integrated Nano, 2024, Vol. 1, Iss. 1, 48-59
DOI: 10.62184/in.jin010420245

Research Article

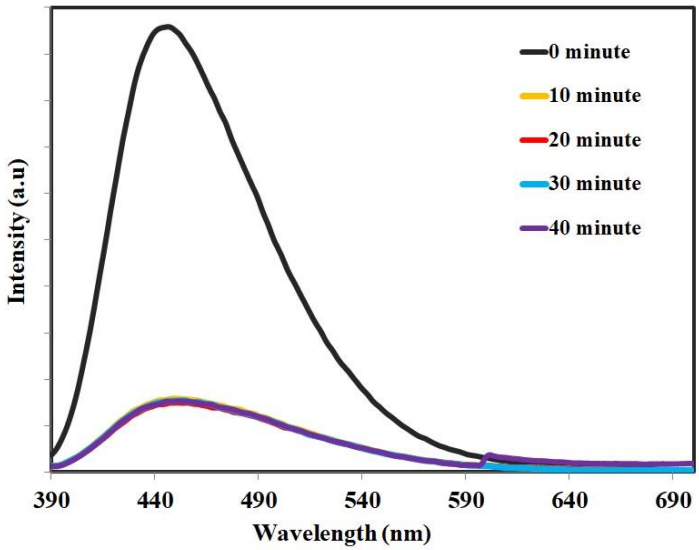

Figure 6. PL spectra of NG/CuInS/ZnS QDs with 500 µM AA at different incubation time.

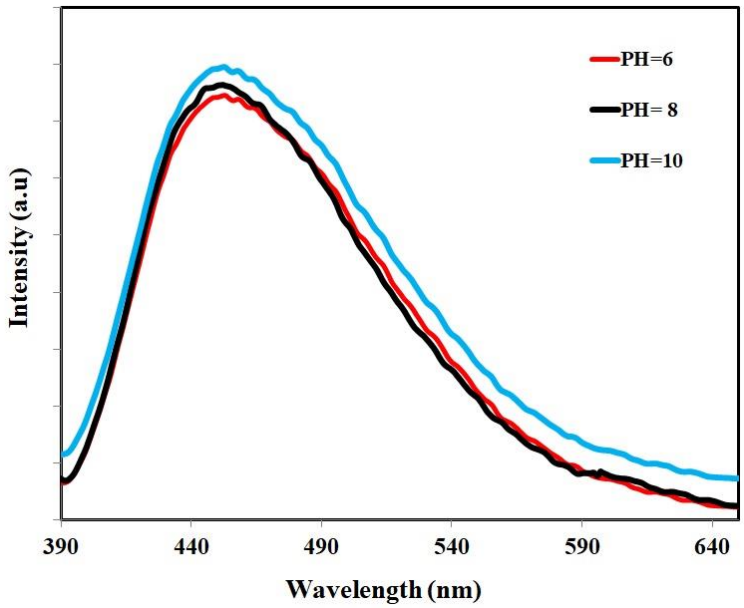

Figure 7. PL spectra of NG/CuInS/ZnS QDs nanocomposite with 500 µM AA at different pH.

3.4.3. Effect of concentration of AA with NG/CuInS/ZnS QDs

PL intensity of NG/CuInS/ZnS QDs with different concentrations of AA from 10 to 500 µM at pH 8 is illustrated in Figure 8. The PL intensity is quenched with increasing the concentration of AA due to electron transfer from QDs to AA. In the inset of Figure 8 the QE vs concentration of AA, the correlation coefficient is found to be 0.9964 and sensitivity is 14 pM^{-1} with a 16.8 µM detection limit compared to other works. It was found that GQDs were used for the detection of AA in the range of 1.11-300 µM and the sensitivity was 49.8 pM^{-1}, and the R^2 was 0.9929 by Liu et al [42]. CuInS QDs for detection AA gave linear in the range of 0.25–200 µM. The detection limit for AA was 0.05 µM and R^2 0.991 by Liu et al. [14].

Integrated Nano, 2024, Vol. 1, Iss. 1, 48-59

DOI: 10.62184/in.jin010420245

Research Article

The oxygen atom's negative charge is spread around the ring. One of its lone pairs interacts with the delocalized electrons on the benzene and ribose rings, creating an extended delocalization that includes the oxygen atom. This stabilizes the enolate intermediate ions, leading to the quenching of the QDs' fluorescence [43-45].

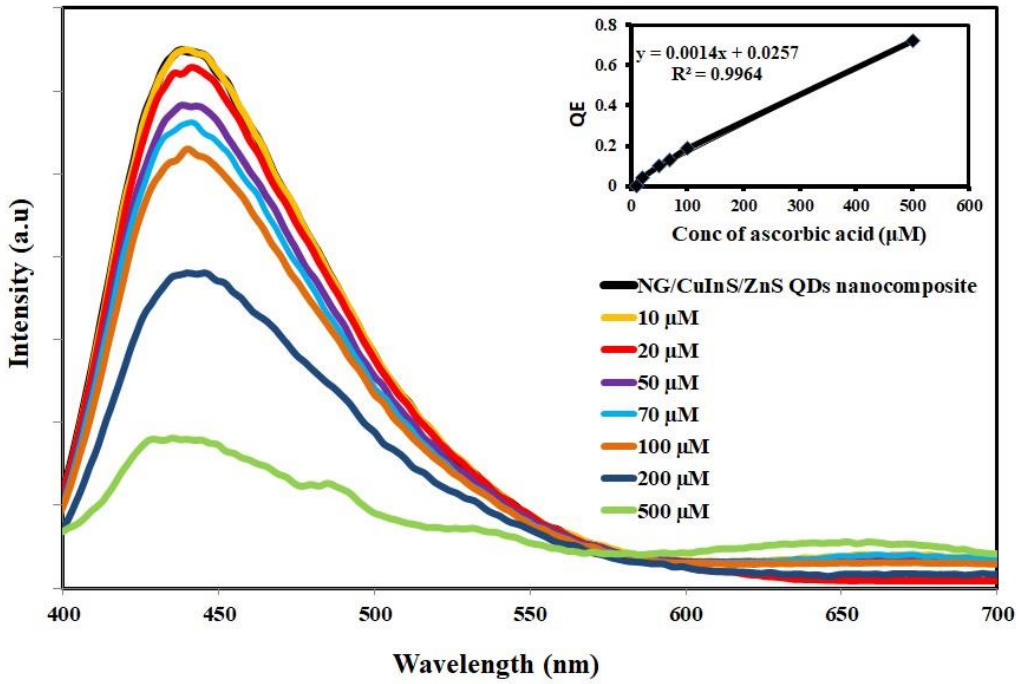

Figure 8. PL spectra of nanocomposite QDs with different concentrations of AA, inset: the QE vs the concentration of AA.

4. Conclusion

In summary, NG/CuInS/ZnS QDs have an excellent downconversion and upconversion PL within the range 443nm, and 650 nm respectively that are synthesized by the reaction of NGQDs with CuInS/ZnS QDs. Ascorbic acid was detected using NG/CuInS/ZnS QDs through PL quenching caused by electron transfer. The NG/CuInS/ZnS QDs' PL intensity was sensitive to pH value. With a limit of detection of 16.8 µM and a correlation coefficient (R^2) of 0.9941, the PL quenching efficiency exhibits a good linear relationship with AA concentration. This demonstrates that NG/CuInS/ZnS QDs can be used to detect AA at the picomolar level easily and sensitively.

Author Information

Corresponding Author: Rania Adel*

E-mail: rania.adel@alexu.edu.eg

References

[1] Gęgotek, A., and Skrzydlewska, E., (2023). Ascorbic acid as antioxidant. Vitamins and Hormones, 121, 247-270. https://doi.org/10.1016/bs.vh.2022.10.008

[2] May, B. M., Parani, S. and Oluwafemi, O. S., (2019). Detection of ascorbic acid using green synthesized $AgInS_2$ quantum dots. Materials Letters, 236, 432-435. https://doi.org/10.1016/j.matlet.2018.10.155

[3] García-Rodríguez, M. del C., Gordillo-García, A. and Altamirano-Lozano, M., (2017). The role of vitamin C in the protection and modulation of genotoxic damage induced by metals associated with oxidative stress. Vitamin C. IntechOpen. Chapter 5, 99. ISBN: 978-938-953-51-3421-3. https://doi.org/10.5772/intechopen.68686

[4] Martynenko, I.V, Litvin, A.P, Purcell-Milton, F, Baranov, A.V, Fedorov, A.V,and Gun'Ko, Y.K., (2017). Application of semiconductor quantum dots in bioimaging and biosensing. Journal of Materials Chemistry, 5(33), 6701-6727. https://doi.org/10.1039/c7tb01425b

[5] Heydari, N, Ghorashi, S.M.B, Han, W, and Park, H.H., (2017) Quantum dot-based light emitting diodes (QDLEDs): New Progress. Quantum-dot Based Light-emitting Diodes. IntechOpen. https://doi.org/10.5772/intechopen.69014

[6] Metwly, W., Fadl, E., Soliman, M., Ebrahim, S., and Sabra, S. A., (2023). Glutathione-capped ZnS Quantum Dots-Urease Conjugate as a highly sensitive urea probe. Journal of Inorganic and Organometallic Polymers and Materials, 33(5), 1388-1399. https://doi.org/10.1007/s10904-023-02592-1

[7] Darsanaki, R.K, Azizzadeh, A, Nourbakhsh, M, Raeisi, G, and, Aliabadi, M.A., (2013). Biosensors: functions and applications. Journal of Biology and Today's World, 2(1), 53-61. https://doi.org/10.15412/J.JBTW.01020105

[8] Chen, F., Yao, Y., Lin, H., Hu, Z., Hu, W., Zang, Z., and, Tang, X., (2018). Synthesis of CuInZnS quantum dots for cell labelling applications. Ceramics International, 44, 34-37. https://doi.org/10.1016/j.ceramint.2018.08.276

[9] Zhang, B., Wang, Y., Yang, C., Hu, S., Gao, Y., Zhang, Y., and Yong, K. T., (2015). The composition effect on the optical properties of aqueous synthesized Cu–In–S and Zn–Cu–In–S quantum dot nanocrystals. Physical Chemistry Chemical Physics, 17(38), 25133-2514. https://doi.org/10.1039/C5CP03312H

[10] Jin, L., Wang, Y., Yan, F., Zhang, J., and, Zhong, F. (2019). The synthesis and application of nitrogen-doped graphene quantum dots on brilliant blue detection. Journal of Nanomaterials, 2019, 1471728. https://doi.org/10.1155/2019/1471728

[11] Rahman, A., Jennings, J. R., & Khan, M. M. (2024). $CuInS_2$ and $CuInS_2$-based nanostructures as photocatalysts. Materials Science in Semiconductor Processing, 169, 107930. https://doi.org/10.1016/j.mssp.2023.107930

[12] Cheong, H. M., Kim, D., Hanna, M. C., and Mascarenhas, A., (2002). Effect of doping on photoluminescence upconversion in GaAs/$Al_x Ga_{1-x} As$ heterostructures. Applied Physics Letters, 81(1), 58-60. https://doi.org/10.1063/1.1491303

[13] Makarov, N. S., Lin, Q., Pietryga, J. M., Robel, I., and Klimov, V. I., (2016). Auger up-conversion of low-intensity infrared light in engineered quantum dots. ACS Nano, 10(12), 10829-10841. https://doi.org/10.1021/acsnano.6b04928

[14] Liu, S., Hu, J., and Su, X., (2012). Detection of ascorbic acid and folic acid based on water-soluble $CuInS_2$ quantum dots. Analyst, 137(19), 4598-4604. https://doi.org/10.1039/c2an35908a

[15] Safardoust-Hojaghan, H., Amiri, O., Hassanpour, M., Panahi-Kalamuei, M., Moayedi, H., and Salavati-Niasari, M., (2019). S, N co-doped graphene quantum dots-induced ascorbic acid fluorescent sensor: Design, characterization and performance. Food Chemistry, 295, 530-536. https://doi.org/10.1016/j.foodchem.2019.05.169

[16] Wang, C., Pan, C., Wei, Z., Wei, X., Yang, F., and Mao, L., (2020). Bionanosensor based on N-doped graphene quantum dots coupled with CoOOH nanosheets and their application for in vivo analysis of ascorbic acid. Analytica Chimica Acta, 1100, 191-199. https://doi.org/10.1016/j.aca.2019.11.008

[17] Kamel, O. A., Fouad, M., and Ali, M., (2023). A Review, Water-Soluble CuInS Quantum Dots, Strategies and Photoluminescence. International Journal of Nanoscience, 22, 2230005. https://doi.org/10.1142/s0219581x2230005x

[18] Li, Y., Zhao, Y., Cheng, H., Hu, Y., Shi, G., Dai, L., and Qu, L., (2012). Nitrogen-doped graphene quantum dots with

oxygen-rich functional groups. Journal of the American Chemical Society, 134(1), 15-18. https://doi.org/10.1021/ja206030c

[19] Zhang, R., Adsetts, J. R., Nie, Y., Sun, X., and Ding, Z., (2018). Electrochemiluminescence of nitrogen-and sulfur-doped graphene quantum dots. Carbon, 129, 45-53. https://doi.org/10.1016/j.carbon.2017.11.091

[20] Bian, H., Wang, Q., Yang, S., Yan, C., Wang, H., Liang, L., and Liu, S. F., (2019). Nitrogen-doped graphene quantum dots for 80% photoluminescence quantum yield for inorganic γ-$CsPbI_3$ perovskite solar cells with efficiency beyond 16%. Journal of Materials Chemistry A, 7(10), 5740-5747. https://doi.org/10.1039/C8TA12519H

[21] Zhou, J., Liu, Y., Tang, J. and Tang, W. (2017). Surface ligands engineering of semiconductor quantum dots for chemosensory and biological applications. Materials Today, 20(7), 360-376. https://doi.org/10.1016/j.mattod.2017.02.006

[22] Adel, R., Ebrahim, S., Shokry, A., Soliman, M., and Khalil, M., (2021). Nanocomposite of CuInS/ZnS and nitrogen-doped graphene quantum dots for cholesterol sensing. ACS omega, 6(3), 2167-2176. https://doi.org/10.1021/acsomega.0c05416

[23] Tian, P., Tang, L., Teng, K. S., and Lau, S. P., (2018). Graphene quantum dots from chemistry to applications. Materials Today Chemistry, 10, 221-258. https://doi.org/10.1016/j.mtchem.2018.09.007

[24] Elkony, Y., Ali, M., Ebrahim, S., and Adel, R., (2022). High photoluminescence polyindole/CuInS quantum dots for Pb ions sensor. Journal of Inorganic and Organometallic Polymers and Materials, 32, 3106-3116. https://doi.org/10.1007/s10904-022-02300-5

[25] Brodie B.C., (1859). XIII. On the atomic weight of graphite. Philosophical Transactions of the Royal Society of London, 149, 249-259. https://doi.org/10.1098/rstl.1859.0013

[26] Liang, Y., Lu, C., Ding, D., Zhao, M., Wang, D., Hu, C. and Tang, Z., (2015). Capping nanoparticles with graphene quantum dots for enhanced thermoelectric performance. Chemical Science, 6, 4103-4108. https://doi.org/10.1039/C5SC00910C

[27] Jiang, Y., Zheng, L., Zheng, H., Wu, F., Shao, L., Zheng, P. and Zhang, Y., (2018). Ultra-highly fluorescent N doped carbon dots-CdTe QDs nanohybrids with excitation-independent emission in the blue-violet region. RSC Advances, 8, 35700-35705. https://doi.org/10.1039/C8RA06326E

[28] Chen, H., Li, W., Zhao, P., Nie, Z. and Yao, S., (2015). A CdTe/CdS quantum dots amplified graphene quantum dots anodic electrochemiluminescence platform and the application for ascorbic acid detection in fruits. Electrochimica Acta, 178, 407-413. https://doi.org/10.1016/j.electacta.2015.08.015

[29] Zhong, Y., Zhang, H., Pan, D., Wang, L. and Zhong, X., (2015). Graphene quantum dots assisted photovoltage and efficiency enhancement in CdSe quantum dot sensitized solar cells. Journal of Energy Chemistry, 24, 722-728. https://doi.org/10.1016/j.jechem.2015.10.006

[30] Rohom, A. B., Londhe, P. U., and Chaure, N. B., (2015). The effect of pH and selenization on the properties of $CuInSe_2$ thin films prepared by electrodeposition technique for device applications. Journal of Solid State Electrochemistry, 19, 201-210. https://doi.org/10.1007/s10008-014-2582-0

[31] Zhuo, S., Shao, M., and Lee, S. T., (2012). Upconversion and downconversion fluorescent graphene quantum dots: ultrasonic preparation and photocatalysis. ACS Nano, 6(2), 1059-1064. https://doi.org/10.1021/nn2040395

[32] Li, M., Wu, W., Ren, W., Cheng, H. M., Tang, N., Zhong, W., and Du, Y., (2012). Synthesis and upconversion luminescence of N-doped graphene quantum dots. Applied

Physics Letters, 101, 103107. https://doi.org/10.1063/1.4750065

[33] Luk, C. M., Tsang, M. K., Chan, C. F., and Lau, S. P., (2014). Two-photon fluorescence in N-doped graphene quantum dots. International Journal of Nuclear and Quantum Engineering, 8, 1387-1390. https://doi.org/10.5281/zenodo.1097427

[34] Feng, Q., Cao, Q., Li, M., Liu, F., Tang, N., and Du, Y., (2013). Synthesis and photoluminescence of fluorinated graphene quantum dots. Applied Physics Letters, 102, 013111. https://doi.org/10.1063/1.4774264

[35] Shen, J., Zhu, Y., Chen, C., Yang, X., and Li, C., (2011). Facile preparation and upconversion luminescence of graphene quantum dots. Chemical Communications, 47, 2580-2582. https://doi.org/10.1039/C0CC04812G

[36] Ke, J., Li, X., Zhao, Q., Liu, B., Liu, S., and Wang, S., (2017). Upconversion carbon quantum dots as visible light responsive component for efficient enhancement of photocatalytic performance. Journal of Colloid and Interface Science, 496, 425-433. https://doi.org/10.1016/j.jcis.2017.01.121

[37] Ning, Z., Molnár, M., Chen, Y., Friberg, P., Gan, L., Ågren, H., and Fu, Y., (2011). Role of surface ligands in optical properties of colloidal CdSe/CdS quantum dots. Physical Chemistry Chemical Physics, 13, 5848-5854. https://doi.org/10.1039/c0cp02688c

[38] Oladeji, I. O., Chow, L., Ferekides, C. S., Viswanathan, V., and Zhao, Z., (2000). Metal/CdTe/CdS/$Cd_{1-x}Zn_xS$/TCO/glass: A new CdTe thin film solar cell structure. Solar Energy Materials and Solar Cells, 61, 203-211. https://doi.org/10.1016/S0927-0248(99)00114-2

[39] Meir, N., Pinkas, I., and Oron, D., (2019). NIR-to-visible upconversion in quantum dots via a ligand induced charge transfer state. RSC Advances, 9, 12153-1216. https://doi.org/10.1039/C9RA01273G

[40] Ali, M., El Nady, J., Ebrahim, S., and Soliman, M., (2018). Structural and optical properties of upconversion CuInS/ZnS quantum dots. Optical Materials, 86, 545-549. https://doi.org/10.1016/j.optmat.2018.10.058

[41] Wen, X., Yu, P., Toh, Y. R., Ma, X., and Tang, J., (2014). On the upconversion fluorescence in carbon nanodots and graphene quantum dots. Chemical Communications, 50, 4703-4706. https://doi.org/10.1039/C4CC01213E

[42] Liu, H., Na, W., Liu, Z., Chen, X., and Su, X., (2017). A novel turn-on fluorescent strategy for sensing ascorbic acid using graphene quantum dots as fluorescent probe. Biosensors and Bioelectronics, 92, 229-233. https://doi.org/10.1016/j.bios.2017.02.005

[43] Li, R., Qi, X., Wu, F., Liu, C., Huang, X., Bai, T., and Xing, S., (2024). Development of a fluorometric and colorimetric dual-mode sensing platform for acid phosphatase assay based on Fe^{3+} functionalized $CuInS_2$/ZnS quantum dots. Analytica Chimica Acta, 1287, 342. https://doi.org/10.1016/j.aca.2023.342121

[44] Ankireddy, S. R., and Kim, J., (2015). Selective detection of dopamine in the presence of ascorbic acid via fluorescence quenching of InP/ZnS quantum dots. International Journal of Nanomedicine, 10, 113. https://doi.org/10.2147/IJN.S88388

[45] Arumugam, N., and Kim, J., (2018). Quantum dots attached to graphene oxide for sensitive detection of ascorbic acid in aqueous solutions. Materials Science and Engineering: C, 92, 720-725. https://doi.org/10.1016/j.msec.2018.07.017